Dynamics of recombination, X inactivation and centromere proteins during stick insect spermatogenesis

Zoé Dumas[1]*, William Toubiana[1]*, Marie Delattre[2], Tanja Schwander[1]

*These authors contributed equally

[1]Department of Ecology and Evolution, University of Lausanne, 1015 Lausanne.

[2]Laboratory of Biology and Modeling of the Cell, Ecole Normale Supérieure de Lyon, CNRS UMR 5239, Inserm U1293, Université Claude Bernard Lyon 1, Lyon, France.

Corresponding authors: william.toubiana@unil.ch, zoe.dumas@unil.ch.

ABSTRACT

In eukaryotes, the cellular processes contributing to gamete formation form the building blocks of genetic inheritance across generations. While traditionally viewed as conserved across model organisms, emerging studies reveal significant variation among eukaryotes in meiotic and post-meiotic processes. Extending our knowledge to non-model organisms is therefore critical to improve our understanding of the evolutionary origin, significance and subsequent modifications associated with gamete formation. We describe the mechanisms underlying recombination, chromosome segregation, and meiotic sex chromosome inactivation in the stick insect group *Timema*. Our results reveal that in males, 1) recombination initiates before synapsis, 2) the mechanisms of X inactivation are variable among species and the X remains silenced despite two waves of transcriptional activation in autosomes during spermatogenesis, 3) chromosome segregation is preceded by the recruitment of centromere proteins that either bind locally or longitudinally along the chromosomes. Together, our observations help understand the evolutionary significance of key cellular processes related to spermatogenesis and shed light on the diversity of their underlying mechanisms among species, including *Timema*.

INTRODUCTION

A key step in sexual reproduction is the generation of haploid cells before fertilization. The transition from diploidy to haploidy is conditioned by meiosis, a cellular process that ensures the maintenance of ploidy levels between generations. During meiosis, chromosomes are inherited from a diploid progenitor germ cell to produce four haploid gametic cells, through two rounds of cell division (1). In males, these events are followed by the process of spermiogenesis, during which the four meiotic products maturate into sperm cells which then fuse with female gametes and restore the diploid cellular state (2). Although meiosis and spermiogenesis are conventionally viewed as highly conserved processes, partly because of conservation in model organisms, an increasing number of studies attest that there is considerable variation among eukaryotes (2-5). Consequently, understanding the diversity of meiotic and post-meiotic processes has become a critical concern for identifying the elements essential for gamete production and elucidating the proximate and ultimate mechanisms underlying the diversification of gametogenesis.

The stick insect genus *Timema* has emerged as a compelling system for exploring the diversity of mechanisms linked to spermatogenesis (i.e., male meiotic and post-meiotic processes), owing to two recently uncovered features during male meiosis (Toubiana and Jeli's papers). First, the chromosomal distribution of the centromere histone determinant CenH3 emerged as particularly dynamic, binding in a localized or chromosome-wide manner depending on chromosomes and meiotic stages (Toubiana et al., 2024). Second, the *Timema*

X chromosome in males, present in a single copy with no homologous Y chromosome (XO system), demonstrated significant alterations in transcriptional activity over gonad development, diminishing in overall gene expression as the meiotic program initiates (Jeli's paper). These findings prompted us to investigate in more detail the cellular processes involved in *Timema* meiosis and their downstream effects during spermiogenesis. While our main focus was on the species *Timema californium*, we also used a comparative approach across different *Timema* species, covering over 30 MY of divergence, and compared our findings with the cellular processes described in other organisms. This approach allowed us to explore the diversity and spatiotemporal dynamics of different mechanisms involved in recombination, meiotic sex chromosome inactivation and chromosome segregation. Overall, our study unveils that despite a conservation in the cytological processes governing sperm formation in *Timema*, the spatiotemporal dynamics of the molecular machinery involved can vary considerably among species, particularly when compared to model organisms.

RESULTS AND DISCUSSION

Timema chromosomes pair and initiate recombination before synapsis during male prophase I

In a canonical depiction of meiosis, the early steps (i.e., prophase I) involve chromosome condensation, pairing, synapsis, and recombination (1). Together, they facilitate the segregation of chromosomes and formation of novel allele combinations (1). However, the temporal and functional relationships between these steps can significantly vary among species. For instance, some lineages exhibit achiasmatic meiosis, where homologous chromosomes segregate without recombination, as it is the case for *Drosophila* males (6). In organisms that do recombine, the link between meiotic recombination and synapsis varies, with dependence or independence of synapsis on the occurrence of double-stranded breaks (DSBs) and recombination (7). These meiotic variants linked to recombination are notably observed in insects, yet because they are difficult to assess without in-depth characterization, only few species have been studied. Consequently, our understanding of the underlying causes and evolutionary patterns behind this diversity remains elusive (6, 8).

We therefore asked whether DSB formation and homologous recombination are required for initiating synapsis during *Timema* male meiosis, which is chiasmatic (9). To this end, we analyzed the temporal localisation of the Double-Stranded Break (DSB) marker γH2AX (a

phosphorylated form of the H2AX histone variant (S139)) and the DNA repair protein Rad51. Progression of synapsis was assessed by the thickening of the cohesin SMC3 filaments, marking the progressive pairing of the SMC3 axes (13). We find that the induction of recombination, including DSB formation and DNA repair mechanisms, starts prior to synapsis, when chromosomes begin to condense and elongate into strands. Indeed, during the late leptotene/early zygotene stages, γH2AX and Rad51 form a cloud of foci at a polarized region of the nucleus (Figure 1; Figure 2). At the same time, thin continuous SMC3 filaments develop and start forming a bouquet configuration (Figure 1; Figure 2; Supplemental figure 3), marking together the condensation of chromosomes via loop extrusion and the clustering of telomeric regions (10, 11).

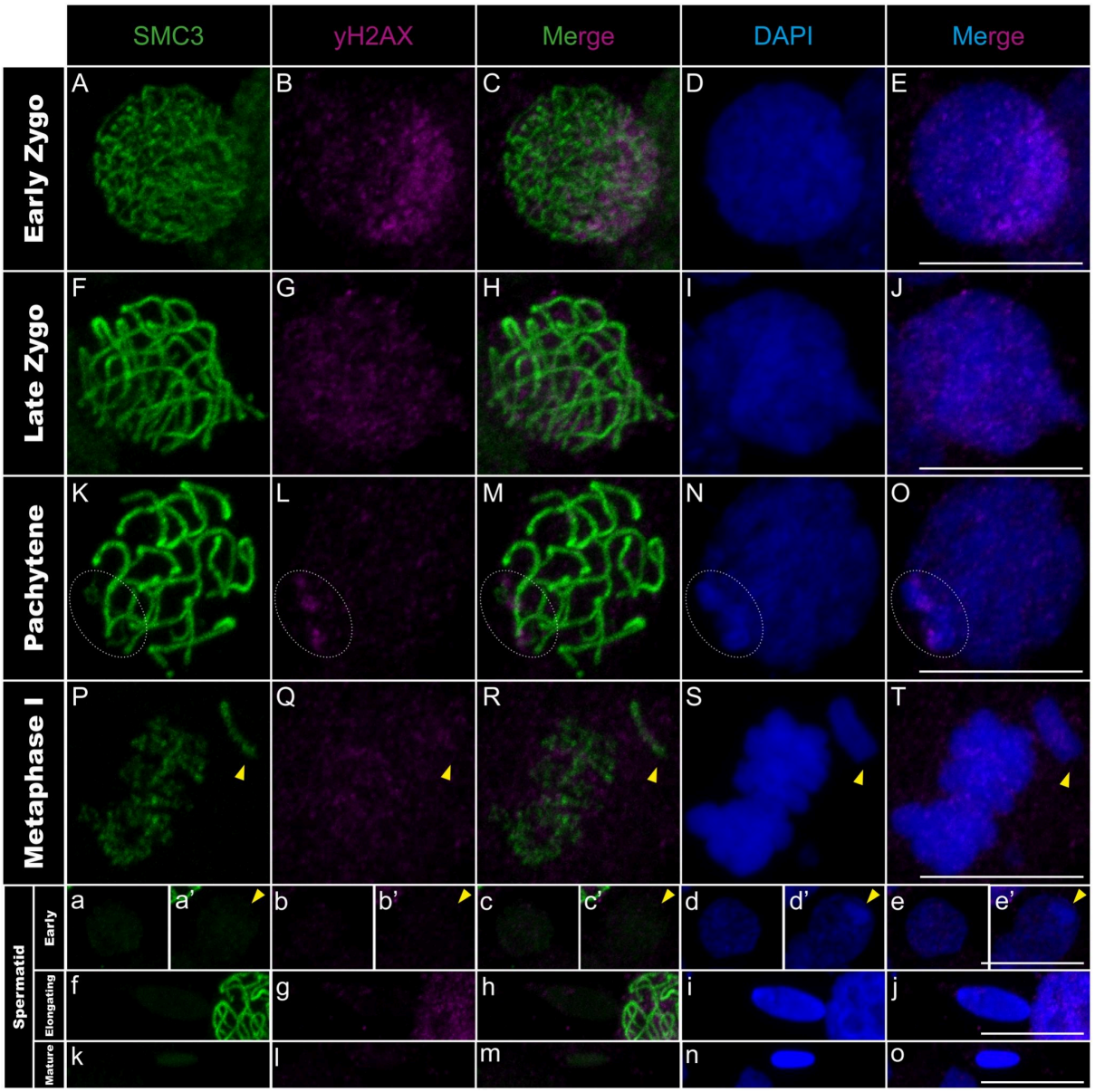

Figure 1: γH2AX distribution in *T. californicum* meiocytes and spermatids. Projections of stack images acquired across *T. californicum* squashed meiocytes (A–T) and spermatids (a–o), at the stages indicated, stained with DAPI (blue) and double immunolabeled for SMC3 (green) and γH2AX (magenta). γH2AX labeling is intense and granular in one nuclear pole, then gradually decreases as synapsis progresses, except on the X chromosome where three patches form in pachytene. The position of the X chromosome is indicated with arrowheads. Scale bar: 10 µm. See Supplemental figure 1 for screens in males of other *Timema* species.

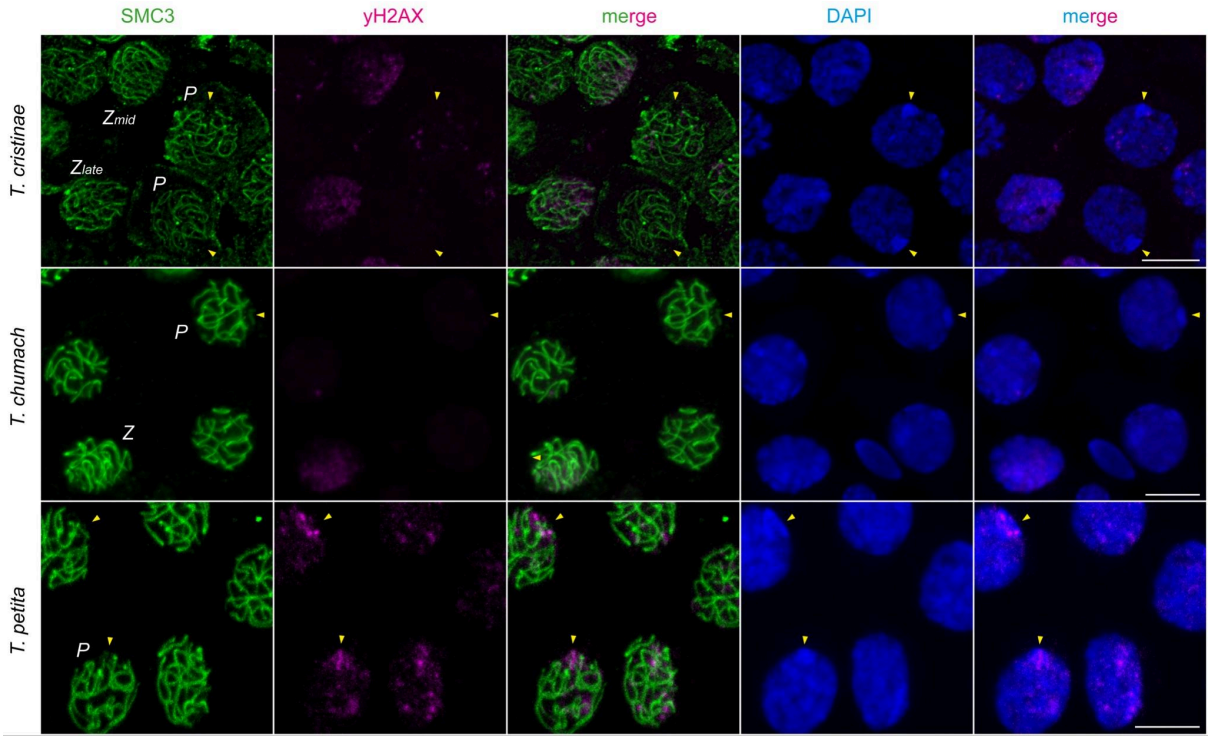

Supplemental figure 1: γH2AX distribution at various stages of spermatogenesis for three additional *Timema* species, acquired through the projection of stack images. Focal cells at the pachytene stage are labeled with the letter *P*, cells at the zygotene stage with the letter *Z*, while yellow arrows indicate the X chromosome. Note that the pachytene X chromosome in *T. petita* displays γH2AX patches as in *T. californicum*, while no signal was detected in *T. cristinae* and *T. chumash* at the same stage. Scale bar: 10 µm

During zygotene, synapsis progresses gradually and asynchronously among chromosomes, alongside with the resolution of the induced DSBs. This was evidenced by SMC3 filaments gradually shifting from thin to thicker filaments, with a variable number of thick filaments among cells, while the γH2AX signal progressively decreases and homogenizes over the entire nuclear surface during the zygotene and pachytene stages (Figure 1; Supplemental figure 2; Supplemental figure 3). Similarly, the Rad51 signal decreases and only a subset of

recombination sites per chromosome persists as discrete foci along SMC3 filaments (Figure 2; Supplemental figure 2). Finally, we observed one to two crossovers per chromosome as indicated by the chromosome shapes as well as shape of SMC3 filaments at metaphase I (Supplemental figure 3). Indeed, metaphase I chromosomes exhibit cross-shaped SMC3 labeling and the formation of "rod" bivalents in all five *Timema* species examined, indicative of a single terminal or sub-terminal chiasmata per chromosome. We also identified three *Timema* species with more circularized SMC3 labeling and the formation of “ring” bivalents, indicative of two terminal or sub-terminal chiasmata, one per chromosome extremity (Supplemental figure 3).

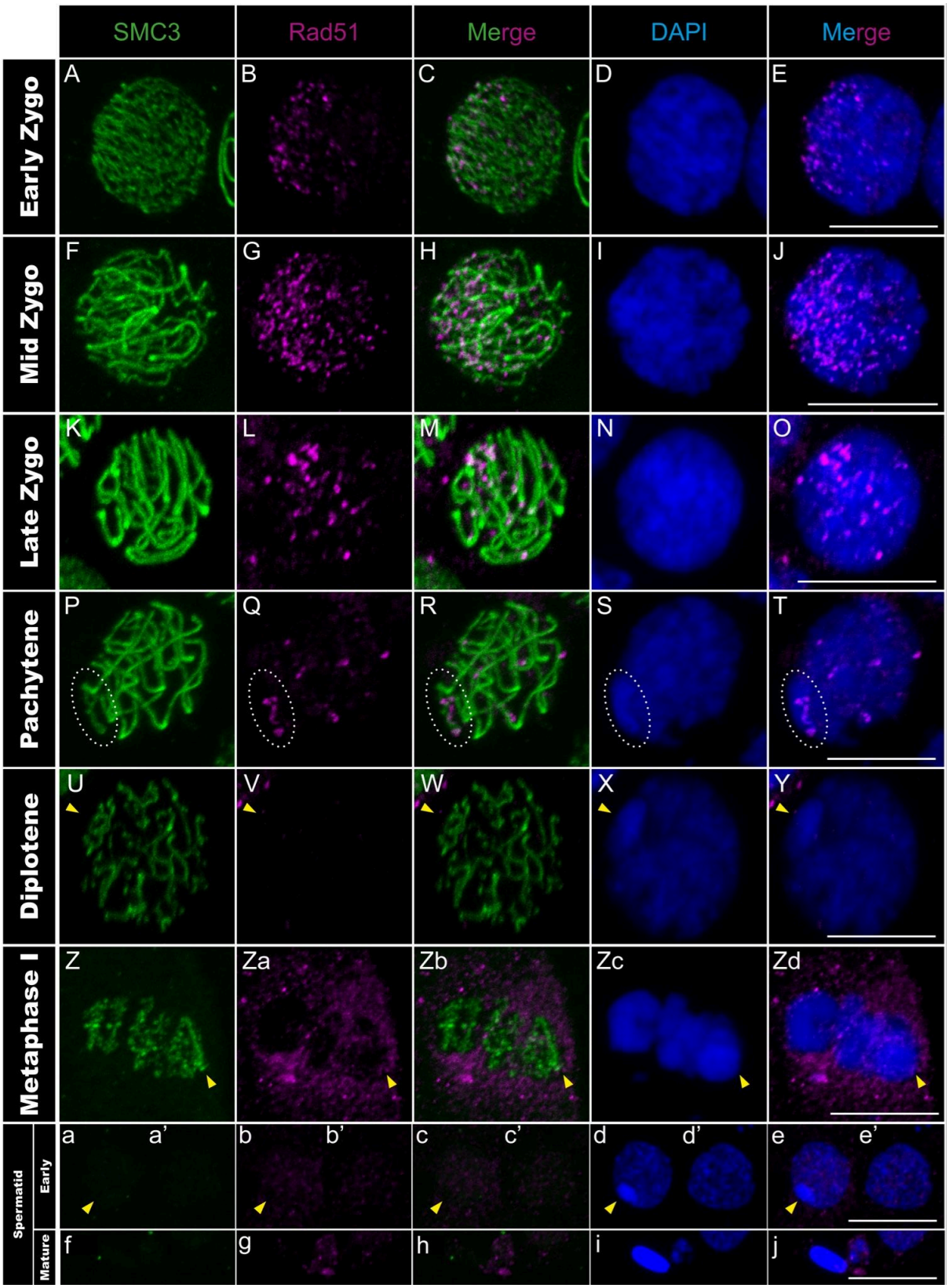

Figure 2: Rad51 distribution in *T. californicum* meiocytes and spermatids. Projections of stack images acquired across *T. californicum* squashed meiocytes (A–Zd) and spermatids (a–o), at the stages

indicated, stained with DAPI (blue) and double immunolabeled for SMC3 (green) and Rad51 (magenta). During the leptotene–zygotene transition, there is an increase in the number of Rad51 foci and a localisation in one nuclear pole, as for γH2AX. As synapsis progresses, the number of Rad51 foci decreases and a few remain on SMC3 axes in pachytene. An accumulation of Rad51 foci on the X chromosome is also observed in pachytene. The position of the X chromosome is indicated with arrowheads and the associated Rad51 signal along its SMC3 axis with dashed circles. Scale bar: 10 µm. See Supplemental figure 2 for screens in males of other *Timema* species.

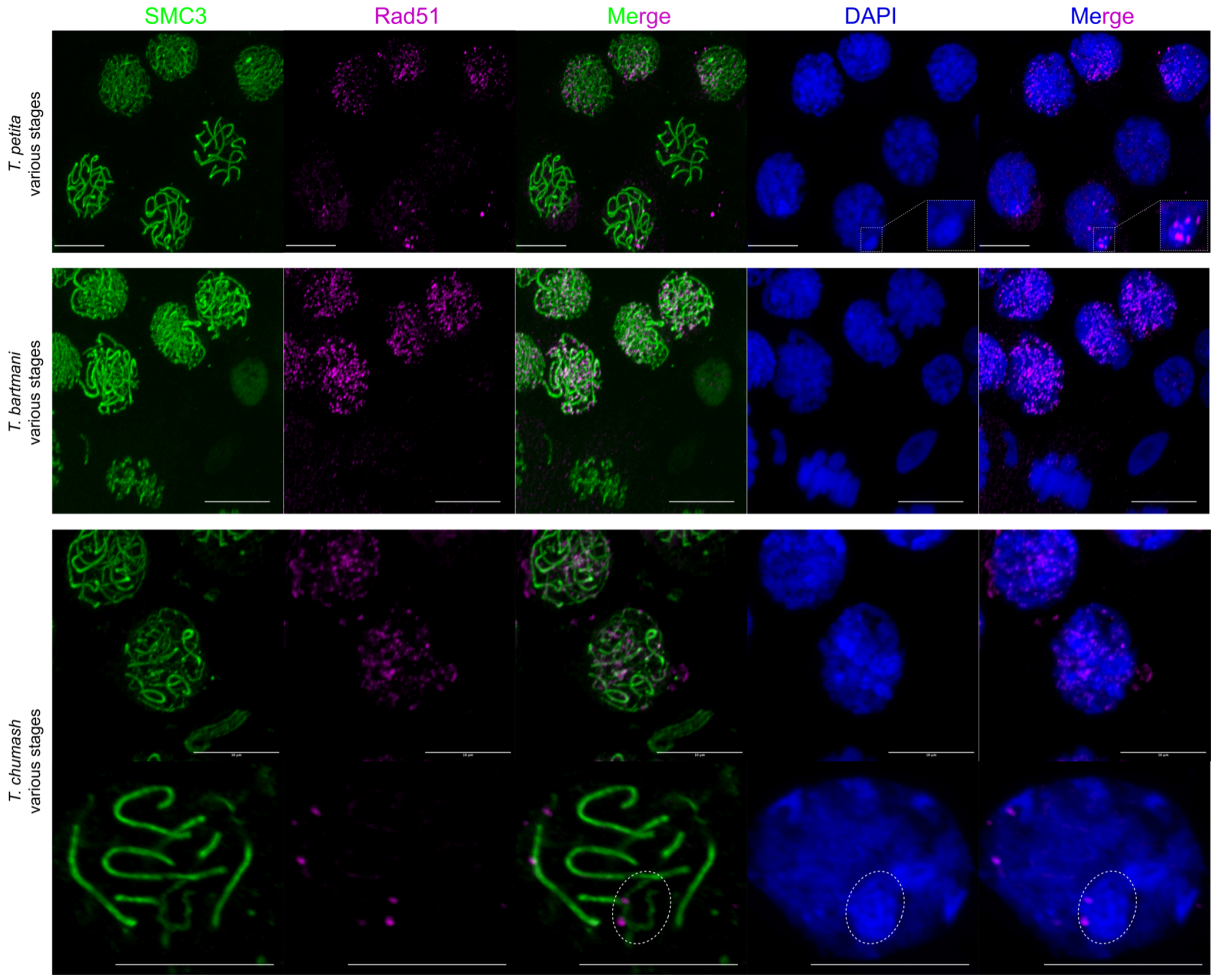

Supplemental figure 2: Rad51 distribution at various stages of spermatogenesis for three additional *Timema* species, acquired through the projection of stack images. Dashed circles and insets indicate

the sex (X) chromosome and the associated Rad51 signal along its SMC3 axis in pachytene. Scale bar: 10 µm.

Overall, our findings show that the phosphorylation of the histone H2AX and the chromosomal deposition of Rad51 occur prior to the thickening of SMC3 filaments, supporting the idea of a recombination-dependent machinery for synapsis formation, as it is the case in *Arabidopsis,* yeast, jellyfish and mouse (12-14). Moreover, we suggest that this functional relationship may reflect the ancestral state in insects. Indeed, only in female meiosis of *Drosophila* (Diptera order) is synapsis known to precede recombination (6, 7). In species of three additional insect orders, meiotic progressions mirror our descriptions in *Timema* in that recombination precedes synapsis (Orthoptera: *Eyprepocnemis plorans* (8, 15); Hemiptera: *Graphosoma italicum* (16); Lepidoptera: *Bombyx mori* (17). Nevertheless, the discrepancy in timing of recombination between *Drosophila* and other insect lineages may also originate from differences in meiotic prophase I between males and females (18, 19). Further studies on female meiosis in additional insect orders will therefore be required before drawing firm conclusions on the evolution of recombination and synapsis in insects.

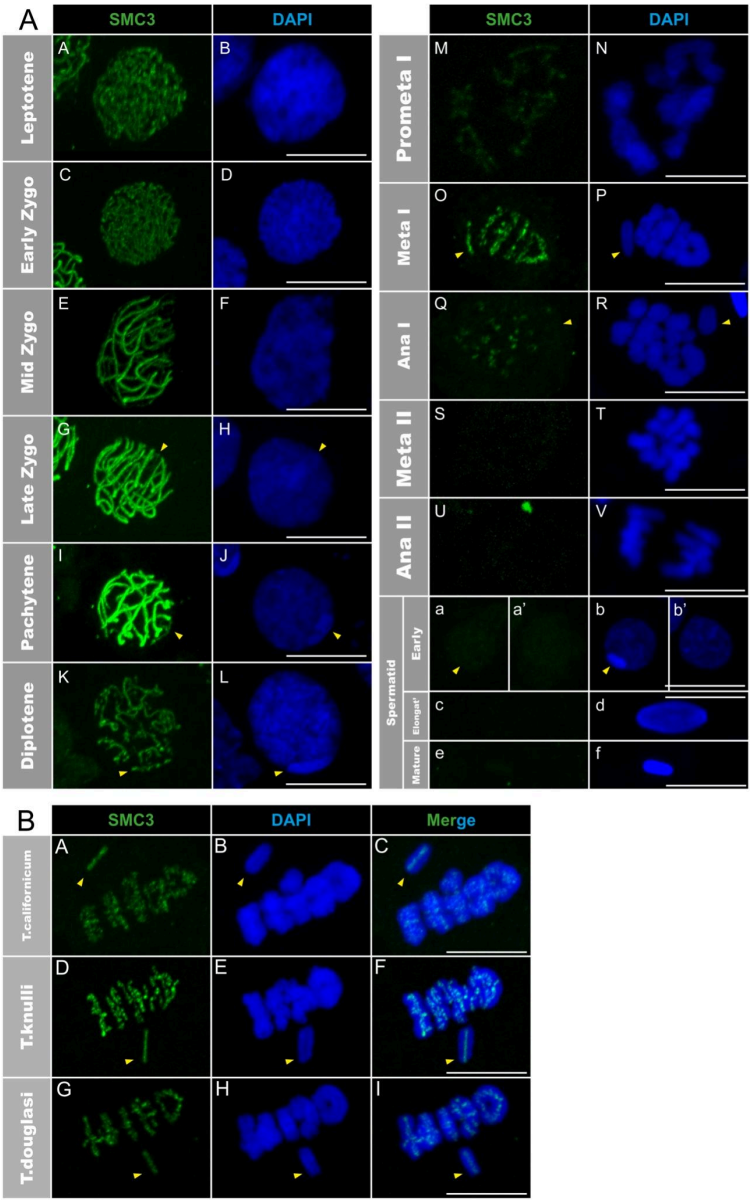

Supplemental figure 3: A) SMC3 distribution throughout *T. californicum* spermatogenesis. While forming thin filaments along chromosomal axes at the onset of meiosis, SMC3 filaments appear thicker as synapsis occurs between homologs. At metaphase I, SMC3 forms cross-shaped or ring-shaped signals corresponding to rod and ring bivalents, respectively. As homologs segregate during anaphase I, SMC3 concentrates into foci near centromeres. SMC3 is then lost from metaphase II onwards. B) Chiasmata across 5 *Timema* species at metaphase I. Note that across many metaphases I analyzed, we observed consistent formation of a large "ring" bivalent in *T. californicum*, *T. knulli* and *T. douglasi* and its absence in *T. podura* and *T. bartmani*. Projections of stack images, scale bar: 10 µm.

Meiotic sex chromosome inactivation in *Timema* males: unique characteristics and spermatogenesis progression

In species with differentiated sex chromosomes such as in X0 or XY systems, sex chromosomes are often associated with major transcriptional changes. Thus, dosage compensation in somatic tissues equalizes transcription levels between the single X copy in males and the two X copies in females (ref). Conversely, in the male germline, sex chromosomes are transcriptionally silenced during meiosis via a process known as meiotic sex chromosome inactivation (MSCI). There is extensive variation in these transcriptional changes among species: for example, dosage compensation can be partial or complete (20) and meiotic sex chromosome inactivation is present in some species but not others (15, 21-24). Furthermore, the precise timing and mechanisms of MSCI appear variable among species, preventing the formulation of a general theory as to why MSCI occurred in the first place (25, 26) (see below for a list of proposed hypotheses). We recently documented that the *Timema* X is initially dosage compensated via upregulation in male gonads, but becomes transcriptionally silenced via MSCI at the onset of meiosis (Jeli's paper). This prompted us to evaluate the cellular dynamics of transcription and MSCI-related mechanisms known in other species (15, 25, 27) throughout *Timema* spermatogenesis.

A key phenotype of MSCI is the intense compaction of sex chromosomes (also termed heteropycnotic or sex body (15, 28)), which is often assisted by the DNA damage response (DDR) pathway. Specifically, sex chromosomes during male meiosis in mammals (particularly

at the pachytene stage) undergo modifications by diverse DDR factors, including γH2AX and Rad-related kinases that accumulate to initiate the chromosome-wide silencing (24, 27). This mechanism is also partially conserved in insects where γH2AX but not Rad51 accumulates on the sex body (15, 29, 30). In *Timema*, our analyses of γH2AX and Rad51 suggest that this cascade has been modified. Indeed, despite the detection of Rad51 proteins as discrete sites along the unsynapsed axial element of the X chromosome (Figure 2), the γH2AX signal is inconsistently detected across *Timema* species during pachytene (Figure 1; Supplemental figure 1). While *T. californicum* and *T. petita* exhibit a few distinct γH2AX patches in X regions, no signal is detected on the X chromosome for *T. cristinae* and *T. chumash*. Importantly, irrespective of this variation between species, the pattern of γH2AX on the *Timema* X chromosome contrasts with the hallmark coat of γH2AX observed on the sex chromosomes of various organisms, including other insects, chicken, marsupials and eutherian mammals (15, 22, 23, 25). Moreover, the X chromosome in all *Timema* species exhibits intense DAPI staining and forms a heteropycnotic body at the nuclear periphery, attesting that the unusual γH2AX pattern does not prevent the tight chromosome compaction associated with MSCI (Figure 1; Supplemental figure 1).

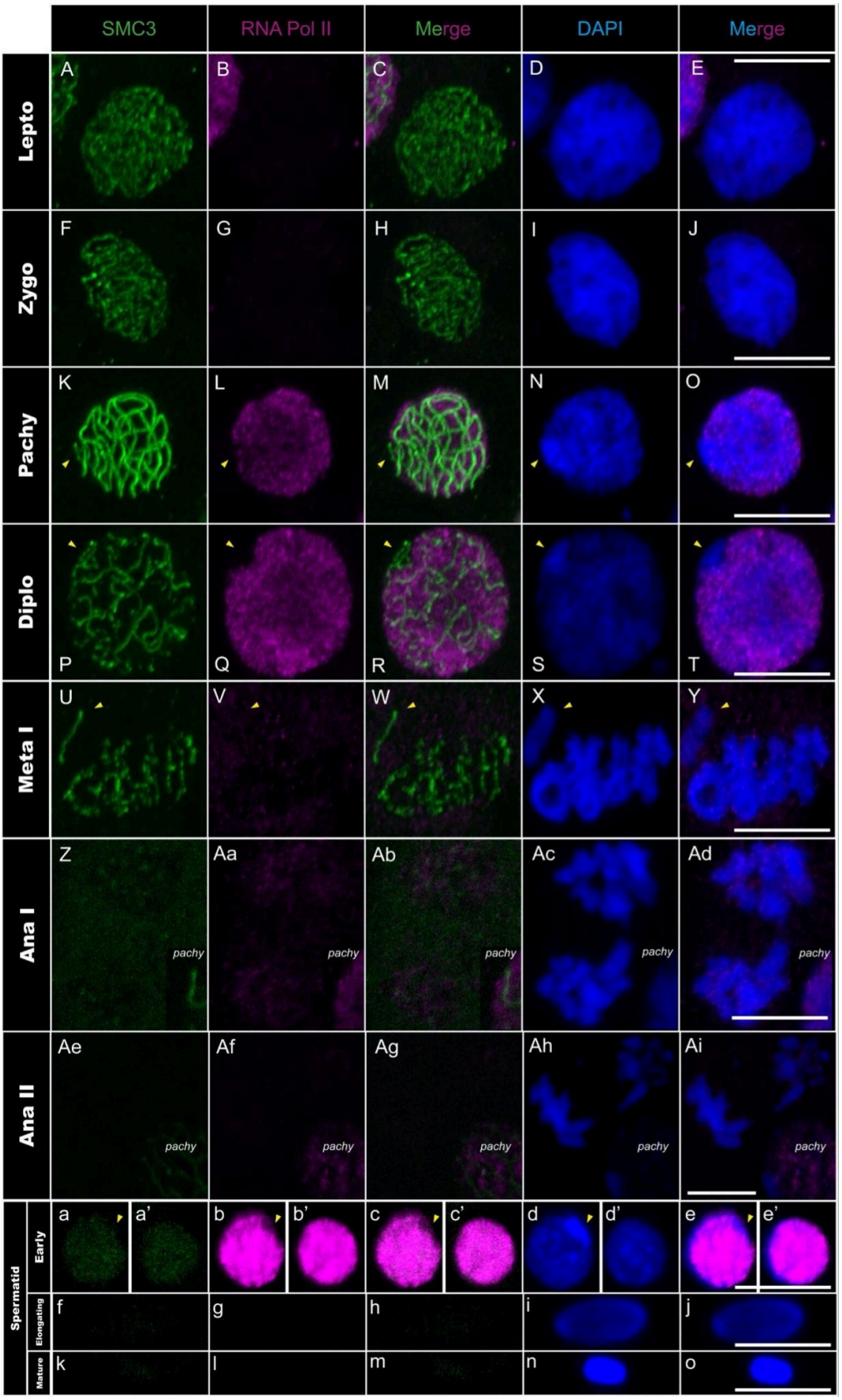

Figure 3: RNApol-II distribution in *T. californicum* meiocytes and spermatids. Projections of stack images acquired across *T. californicum* squashed meiocytes (A–Ad) and spermatids (a–o), at the

stages indicated, stained with DAPI (blue) and double immunolabeled for SMC3 (green) and RNApol-II (magenta). RNApol-II labeling is intense from pachytene to diplotene, and in the round spermatid stage. During all spermatogenesis stages, the X chromosome is extremely reduced in RNApol-II labeling. The position of the sex (X) chromosome is indicated with arrowheads. Scale bar: 10 µm.

We then investigated whether the X chromosome in *Timema* was transcriptionally inactive throughout spermatogenesis or only at specific stages. We found that the X chromosome remains transcriptionally inactive throughout spermatogenesis, while there are two phases of autosomal transcription during meiosis and spermiogenesis. Indeed, the RNA polymerase II signal is completely absent from the entire nucleus at the onset of prophase I (i.e., leptotene and zygotene stages; Figure 3). It then appears at the pachytene stage on the autosomes, concomitantly with the formation of the heteropycnotic body and accumulation of Rad51 proteins on the X (Figure 2; Supplementary figure 2; Figure 3). At this same stage, the X chromosome becomes coated by the modified histone H3K9me3 (Figure 4; Supplemental figure 4), a heterochromatin hallmark involved in transcriptional repression and heteropycnotic body formation during MSCI (15, 27). However, while the heteropycnotic body persists in all species until the round spermatid stage, the maintenance of H3K9me3 on the X varies among species: it remains until the round spermatid stage in *T. petita* and *T. chumash* whereas its signal is already lost at this stage in *T. californicum* and *T. cristinae* (Figure 4; Supplemental figure 4). Independently of the H3K9me3 signal in each species, a second transcriptional phase also occurs at this stage, once again characterized by an

intense RNA polymerase II signal on the autosomes but not the X chromosome (Figure 3; Figure 4; Supplemental figure 4). As spermatids then elongate, the polymerase II signal is depleted from the nuclei and the heteropycnotic body is no longer visible (Figure 3; Figure 4; Supplemental figure 4).

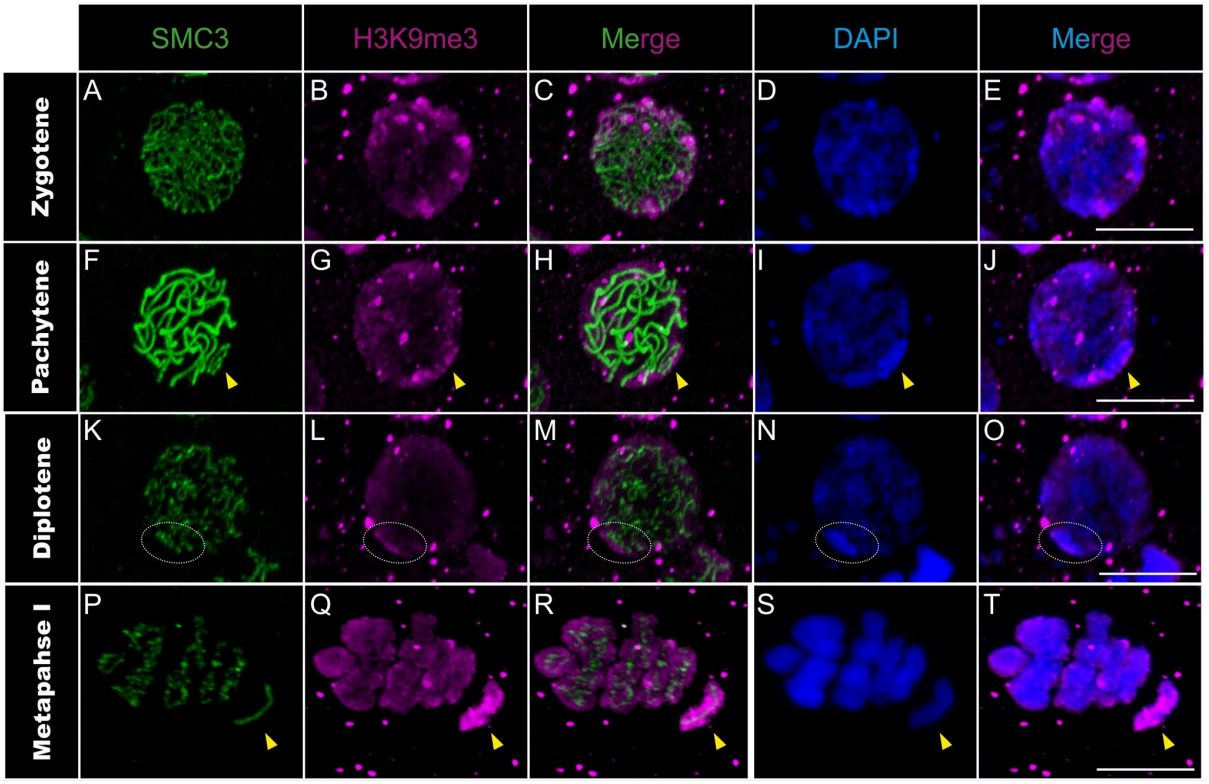

Figure 4: H3K9me3 distribution in *T. californicum* meiocytes. Projections of stack images acquired across *T. californicum* squashed meiocytes (A–T) at the stages indicated, stained with DAPI (blue) and double immunolabeled for SMC3 (green) and H3K9me3 (magenta). H3K9me3 labeling is particularly intense, coating the X chromosome from the pachytene stage. During spermiogenesis, H3K9me3 signal is absent on the X chromosome. The position of the sex (X) chromosome is indicated with arrowheads and the associated H3K9me3 signal with dashed circles. Scale bar: 10 µm.

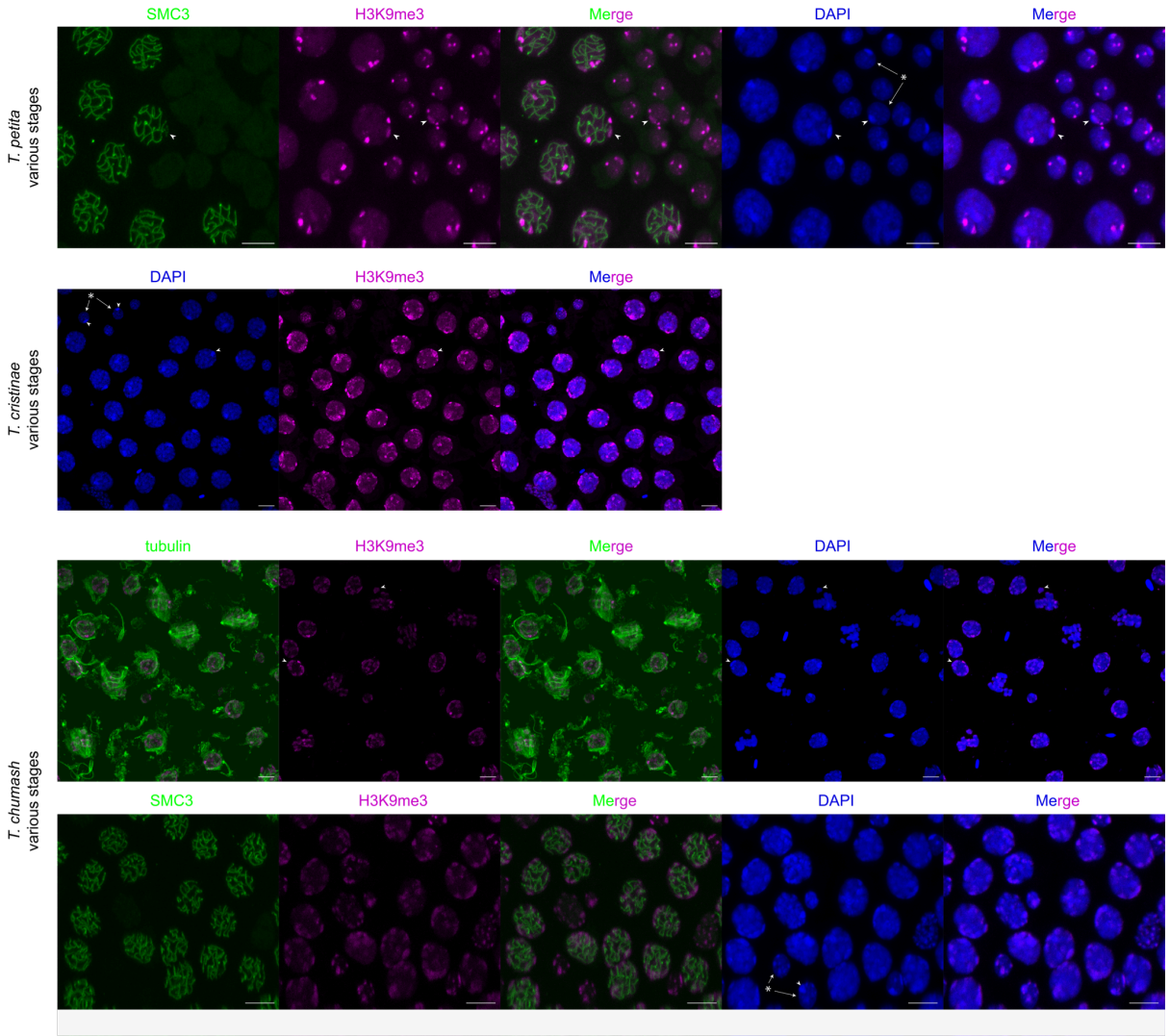

Supplemental figure 4: H3K9me3 distribution at various stages of spermatogenesis for three additional species, acquired through the projection of stack images. Note the presence of H3K9me3 coating the X chromosome in round spermatids in *T. petita* and *T. chumash* but not in *T. cristinae*. Arrowheads indicate the location of the X chromosome. Asterisks indicate round spermatids. Scale bar: 10 µm.

Combined, our findings show that the complete transcriptional inactivity of the X chromosome throughout *Timema* spermatogenesis involves a series of intricate mechanisms that can be decomposed into five distinct cellular steps. During the first step, the polymerase

II and MSCI markers are absent from nuclei in leptotene and zygotene stages, and all chromosomes, including the X chromosome, are most likely transcriptionally inactive. The second step involves the formation of a heteropycnotic body along with the appearance of MSCI markers and the maintenance of a transcriptionally silenced X from pachytene to diplotene, while autosomes undergo a first wave of transcription. Importantly, this step seems to require the presence of Rad51 (as in mammals but not in two other insect species (21, 29, 34)) and does not seem to necessitate the accumulation of γH2AX on the X chromosome (as in mammals and grasshoppers (29, 34)). In the third step, transcription is again strongly reduced or completely lacking during metaphase I, while the X chromosome maintains the H3K9me3 modification in all species. The fourth step marks the presence of the heteropycnotic body until the round spermatid stage and the initiation of the second wave of autosomal transcription. This step is also marked by some variation in the maintenance of H3K9me3 among *Timema* species, indicating that this epigenetic modification is not essential for the maintenance of X silencing at this stage. Finally, the fifth and last step involves the loss of MSCI and transcriptional markers in all species as spermatids elongate and maturate.

The mechanisms engaged in MSCI in *Timema* offer a new perspective on the driving forces behind the origin of the process. The evolution and key function of MSCI continues to be a source of theories and speculations, with different proximate and ultimate hypotheses proposed.

A first hypothesis posits that MSCI primarily operates to shelter unsynapsed region(s) on the sex chromosomes during the first meiotic division. Indeed, different factors may be required for such sheltering, including damaging effects of unrepaired DSBs or ectopic recombination as well as circumventing cellular checkpoints that are active during prophase I (27, 31, 32). Our findings allow us to exclude at least two such factors. First, MSCI does not appear necessary to shelter the X from the induction of DSBs during meiosis in *Timema*. Indeed, MSCI begins at a later stage than the initiation of DSBs (illustrated by the phosphorylation of H2AX in leptotene), meaning that MSCI cannot protect the X from the induction of DSBs. This contrasts with findings in other species such as the grasshopper *Eyprepocnemis plorans* where MSCI establishment precedes the γH2AX signal on the X (20). Our observations in *Timema* thus suggest that unrepaired DSBs may not be the primary factors involved in MSCI. Secondly, MSCI does not solely serve to circumvent checkpoints during meiosis. This is revealed by the fact that the *Timema* X chromosome maintains its condensation state and transcriptional inactivation long after the first meiotic division (i.e., until spermiogenesis and significantly past putative checkpoints), suggesting that other factors are involved in maintaining the X transcriptionally silenced.

A second, mutually non-exclusive hypothesis postulates that MSCI functions to transcriptionally silence some or all genes on the sex chromosomes that could impact cell survival during various stages of spermatogenesis and post-spermatogenesis (25, 31). Our investigation of MSCI in *Timema* supports this hypothesis, revealing first that the X chromosome remains silent throughout meiosis and MSCI markers emerge only when

meiotic transcription activates in pachytene. Similarly, we identified in the literature that MSCI markers are typically found in species such as mice, opossum or grasshoppers, where transcription activates during meiosis (15, 23, 24), while MSCI markers appear to be absent in species such as platypus or chicken, where global transcription is low during meiosis (21, 22). In *Timema*, we further show that a transcriptional activity post-meiosis is sufficient to explain the maintenance of the X-silencing status until the round spermatid stage. Indeed, during this cell stage, a transcription of X-linked genes would be expected to result in major expression differences between nullo-X and X-containing spermatids. Our interpretations are again supported by findings in mice, opossum or grasshoppers, which are also characterized by transcriptional repression of sex chromosomes post-meiosis (also termed postmeiotic sex chromatin (PMSC)) (15, 23, 25, 33).

Overall, the cell biology of MSCI in *Timema*, indicates that a hypothesis based on the sheltering of unsynapsed chromosomes during meiosis I is not sufficient to fully explain MSCI and that active repression of sex-linked genes throughout spermatogenesis likely plays an important role.

Dynamics and assembly of centromere proteins during spermatogenesis

The absence of transcription from autosomes and the X chromosome during leptotene and zygotene in meiosis I (Figure 3) coincides with the recruitment of the centromere histone

variant CenH3 along the full length of all chromosomes, an unexpected phenotype which we described recently (Toubiana et al 2024) (Figure 5). Indeed, in species with monocentric chromosomes such as *Timema*, CenH3 is expected to localize to confined chromosomal regions to which other centromere proteins are then recruited to ensure proper segregation during cell division (34). On the other hand, a longitudinal distribution of CenH3 is typically characteristic of species with holocentric chromosomes (35). During the transition from zygotene to pachytene, *Timema* establishes the expected monocentric distribution of CenH3 on the autosomes but not on the X (Toubiana 2024), which we here show occurs in parallel to the activation of transcription from the autosomes and silencing of the X (Figure 3; Figure 5). We thus extended our previous observations of CenH3 to include additional stages of spermatogenesis and centromere proteins to probe for a broader correlation between transcription and centromere protein recruitments as seen in *C. elegans* (36) and some Lepidoptera (37), as well as to integrate the recruitment dynamics of CenH3 and other centromere proteins with spermatogenesis progression.

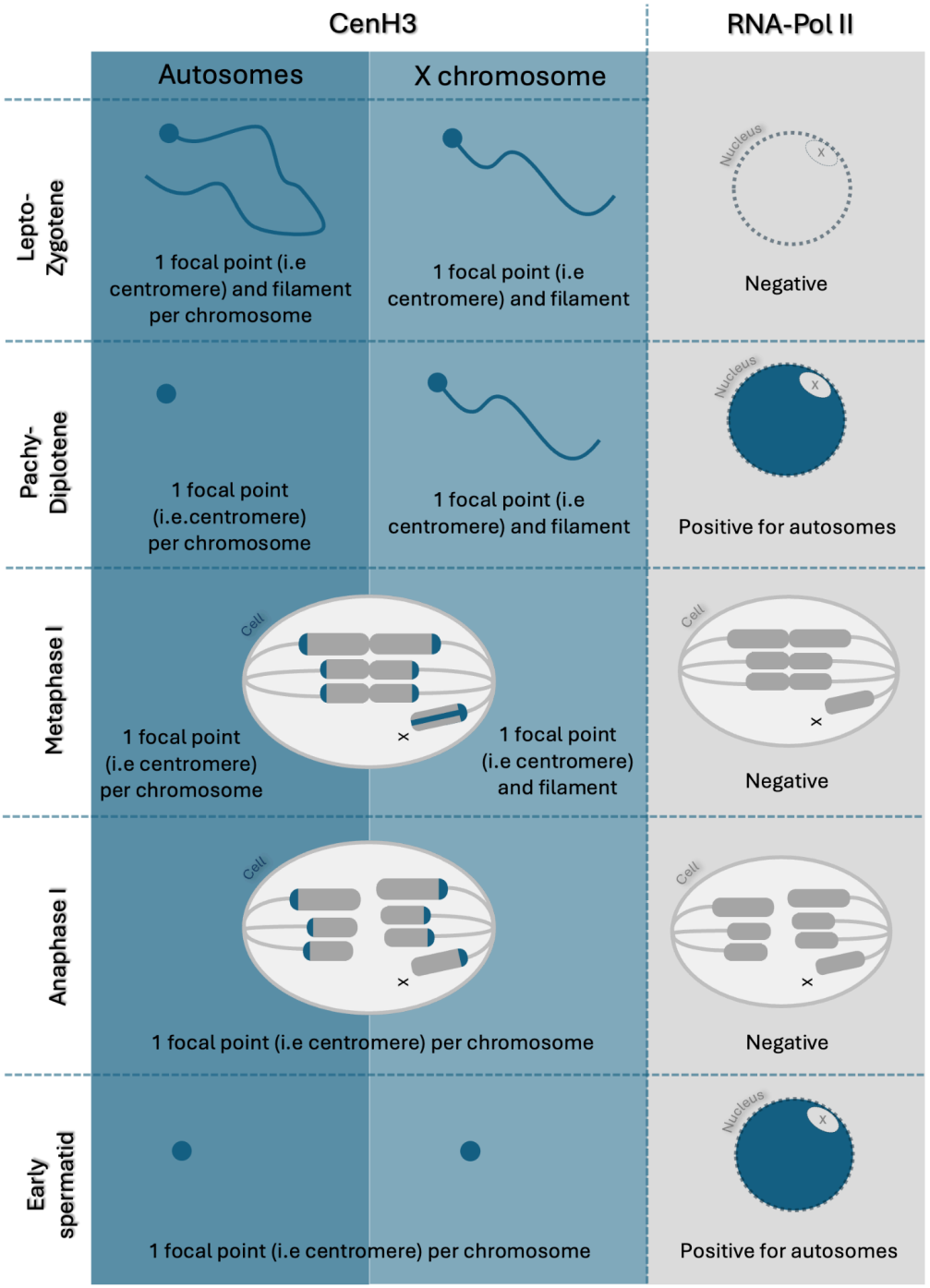

Figure 5: Schematic representation of CenH3 and RNApol-II distributions across different stages of spermatogenesis in *Timema*. The first activation of transcription in autosomes coincides with the removal of CenH3 along these chromosomes. However, the removal of CenH3 along the X chromosome does not correlate with an activation of transcription on this chromosome.

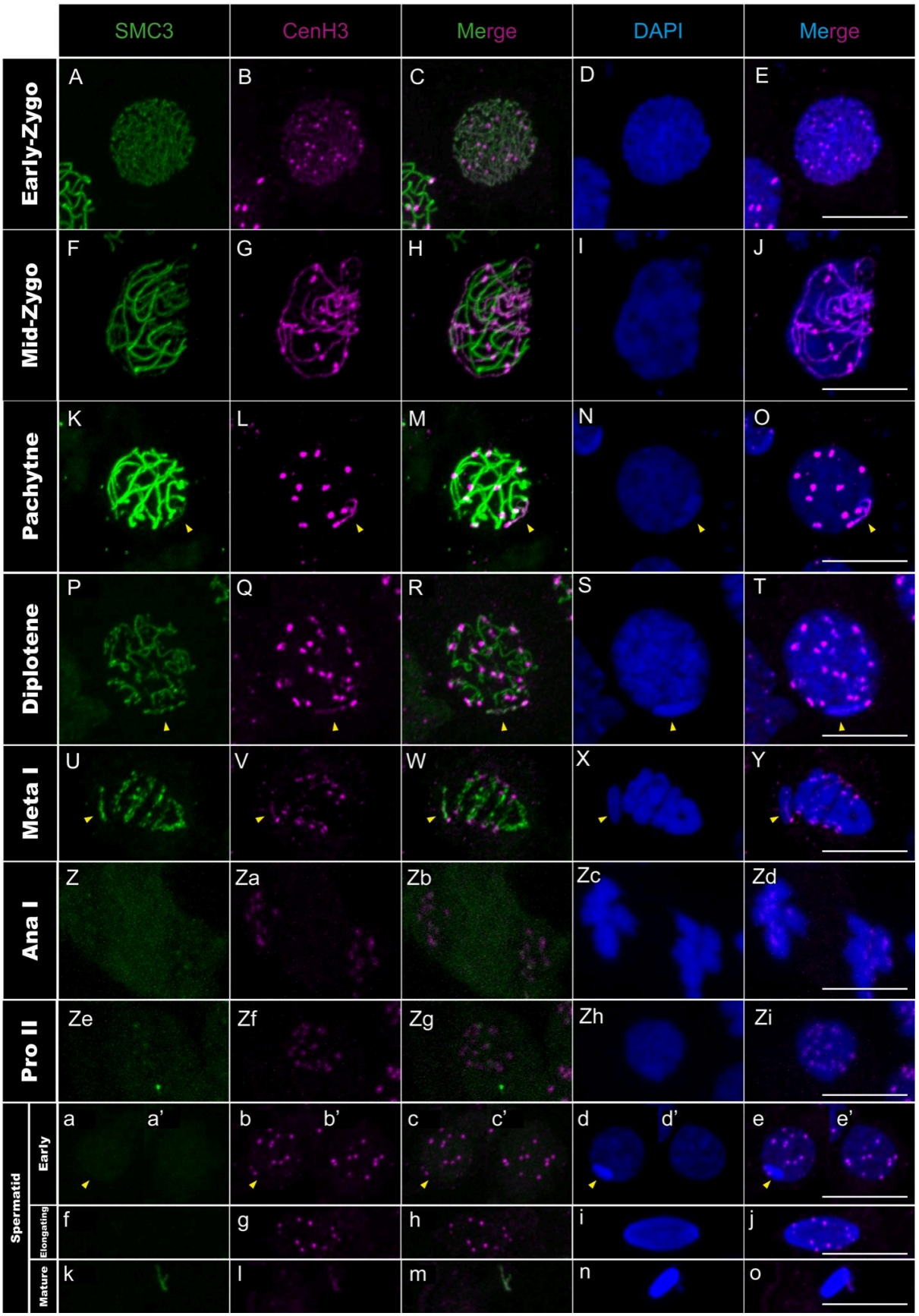

Figure 6: CenH3 distribution in *T. californicum* meiocytes and spermatids. Projections of stack images

acquired across *T. californicum* squashed meiocytes (A–Zi) and spermatids (a–o), at the stages indicated, stained with DAPI (blue) and double immunolabeled for SMC3 (green) and CenH3 (magenta). While CenH3 is distributed along chromosomal axes at the onset of meiosis (leptotene and early zygotene), it becomes restricted to foci, first in autosomes as synapsis progresses (from mid-zygotene to metaphase I), then also in X chromosome from anaphase I. The position of the sex (X) chromosome is indicated with arrowheads. Scale bar: 10 µm.

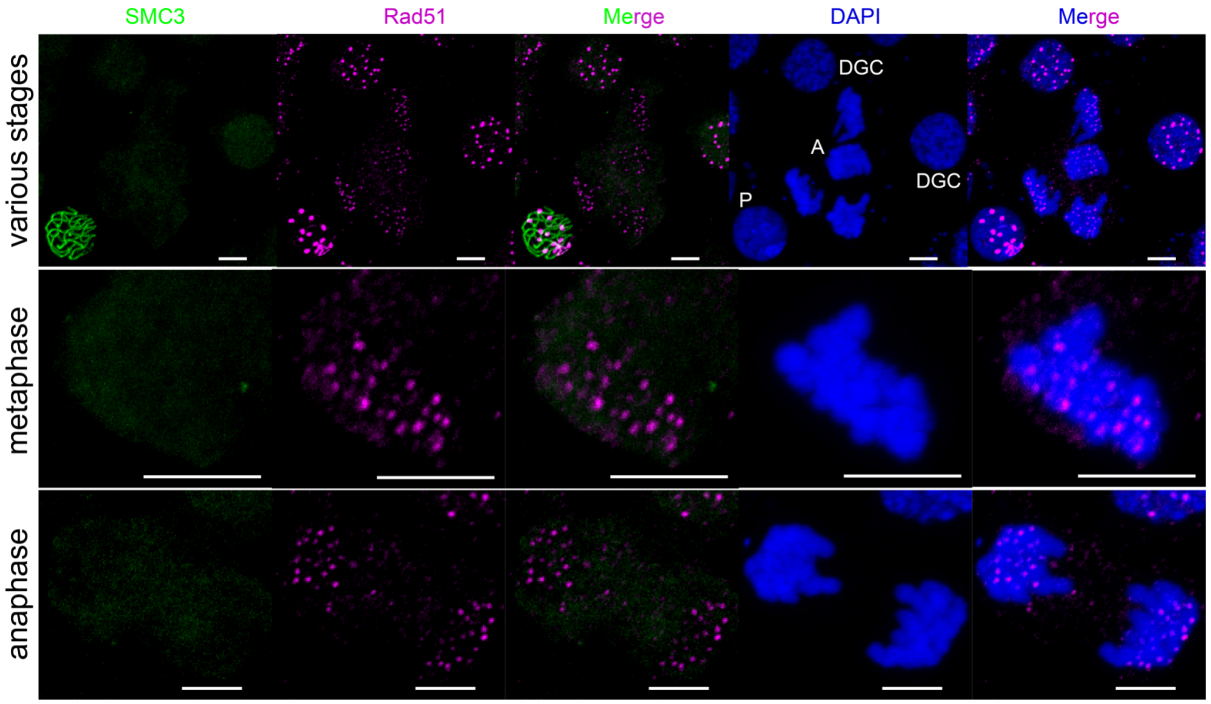

Supplemental figure 5: CenH3 distribution in germ cells of *T. californicum* male gonads. The upper panel contrasts the distribution of CenH3 for cells in meiosis ("P" for Pachytene) and before entering meiosis ("DGC" for Diploid Germ Cell and "A" for Anaphase). A zoom on germ cells in metaphase and anaphase is shown in the two other panels, where CenH3 is restricted to foci. Scale bar: 5 µm.

We first identified that CenH3 distributes in single foci on every chromosome in male mitotic gonadal cells (Supplemental figure 5). Once meiosis initiates (i.e., lepto- to zygotene stage),

CenH3 is recruited over the entire length of every chromosome in all *Timema* species (Figure 6; Supplementary figure 6; see Figure 6 legend for more details of the CenH3 dynamics throughout prophase I), confirming our previous observations (Toubiana et al. 2024). Following the first meiotic division, the longitudinal distribution of CenH3 along the X chromosome then disappears to form a single focus on the X (i.e., the expected monocentric distribution; Figure 6). Contrary to the shift from longitudinal to monocentric distribution of CenH3 on the autosomes, the shift of CenH3 on the X is not accompanied by an activation of transcription on this chromosome, as the X remains silenced beyond the first meiotic division (Figure 3; Figure 6). Thus, although the distribution dynamics of CenH3 can be explained by the dynamics of transcription on the autosomes, the loss of its longitudinal distribution on the X from anaphase I onwards is not supported by a transcriptional activation of the X (Figure 5). Finally, we noticed that the CenH3 signal is completely lost from all chromosomes at the stage of mature sperms (Figure 6; Supplementary figure 6), which is either caused by an active removal of the protein as in *Drosophila virilis* and *Caenorhabditis elegans* (36, 38), or because the chromatin is too compacted at this stage for antibody accessibility.

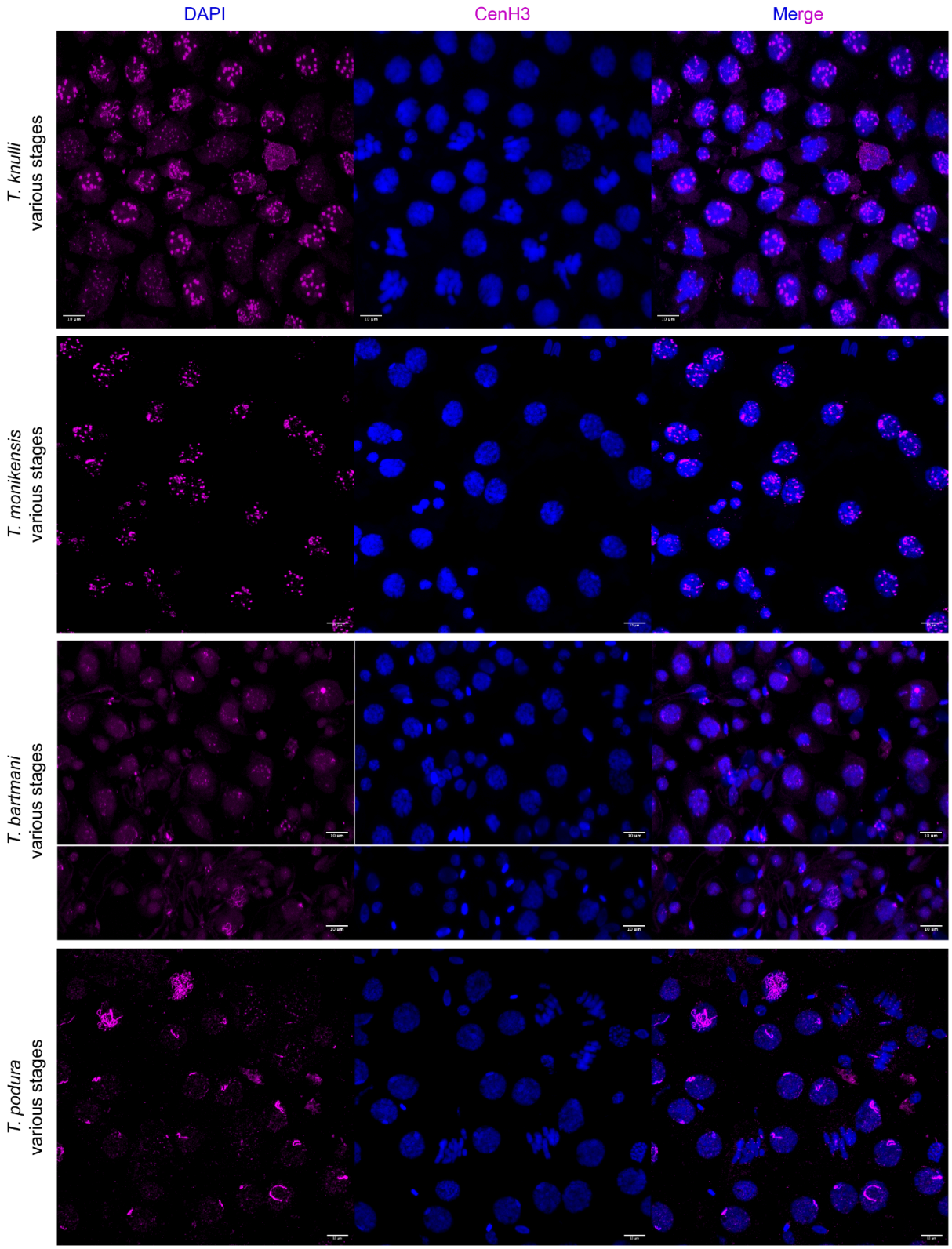

Supplemental figure 6: CenH3 distribution in various stages of spermatogenesis for four additional species, acquired through the projection of stack images. Scale bar: 10 µm.

The different distributions of CenH3 along chromosomes in *Timema* (i.e., longitudinal or restricted to monocentric foci) raises the question which mechanisms govern its deposition onto chromosomes. In holocentric lineages, in addition to the role of transcription, recent modeling efforts to understand the assembly of centromeric nucleosomes into longitudinal holocentromeres have proposed that blocking and anchoring interactions between centromeric nucleosomes and SMC proteins during loop extrusion could yield a holocentric-like chromosome via chromatin condensation (39). Our observed dynamics of CenH3 in male gonadal cells closely match these model predictions. First, CenH3 filaments form when loop extrusion initiates and SMC3 proteins run along the length of every chromosome during leptotene. Second, the CenH3 filament on the X chromosome disappears when the cohesin axis retires from chromosome arms' length in anaphase I.

In monocentric lineages, CenH3 is deposited exclusively to active centromeres through a complex deposition network. This network entails a cascade of proteins either employed in remodeling chromatin structure to prepare for CenH3 deposition or interacting with CenH3, itself, to facilitate its deposition (40). Among others, certain centromere proteins, such as the kinetochore protein CenpC, appear to play an important role in recruiting CenH3 during both mitosis and meiosis, as it is the case in chicken, human or *Drosophila* (41, 42). Hence, there seems to be an interplay among centromere proteins, whereby CenH3 can recruit the same proteins that facilitate its deposition onto the DNA (34, 41-44).

To develop insights into the interplay between CenH3 dynamics and these centromere proteins in *Timema*, we focused on the cytological characterization of two kinetochore

proteins and one spindle assembly checkpoint (SAC) protein (43-45). We first investigated the dynamics and chromosomal distribution of the CenpC protein, a protein from the inner kinetochore complex, while testing the hypothesis that this protein may be involved in the longitudinal recruitment of CenH3 (41, 43). Our observations indicated that CenpC is absent at early prophase stages (i.e. lepto- and zygotene stages) and binds in a monocentric fashion on all chromosomes from pachytene until the end of the first meiotic division, making the hypothesis of the longitudinal CenH3 recruitment unlikely (Figure 7; Supplemental figure 7).

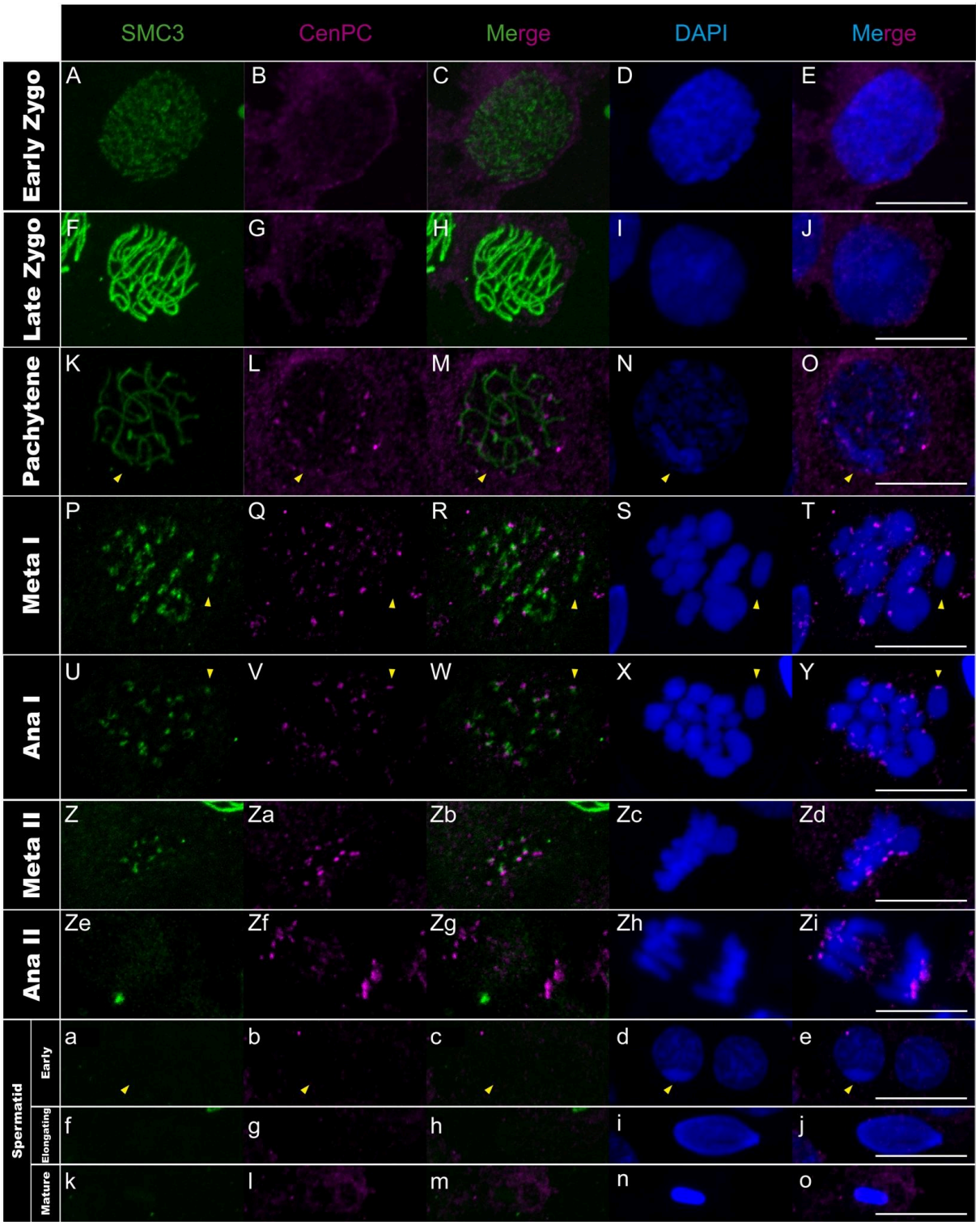

Figure 7: CenpC distribution in *T. californicum* meiocytes and spermatids. Projections of stack images acquired across *T. californicum* squashed meiocytes (A–Zn) and spermatids (a–o), at the stages indicated, stained with DAPI (blue) and double immunolabeled for SMC3 (green) and CenpC (magenta). The CenpC signal is not detected until the pachytene stage where it is distributed in foci

on every chromosome until anaphase II. The CenpC signal is then lost at the onset of spermiogenesis. The position of the sex (X) chromosome is indicated with arrowheads. Scale bar: 10 µm.

Supplemental figure 7: CenpC distribution at various stages of spermatogenesis for two additional species, acquired through the projection of stack images. Scale bar: 10 µm.

We then examined the cellular patterns of the outer kinetochore protein Ndc80 and SAC protein Bub1, but both are absent during prophase I. They load in monocentric fashion on every chromosome only at pro-metaphase 1, when the nuclear membrane disassembles (Figure 8; Figure 9; Supplemental figure 8; Supplemental figure 9). This pattern confirmed the idea that the assembly of the outer kinetochore region is tightly regulated in time, taking place just before segregation to prevent premature microtubule–kinetochore interactions (46).

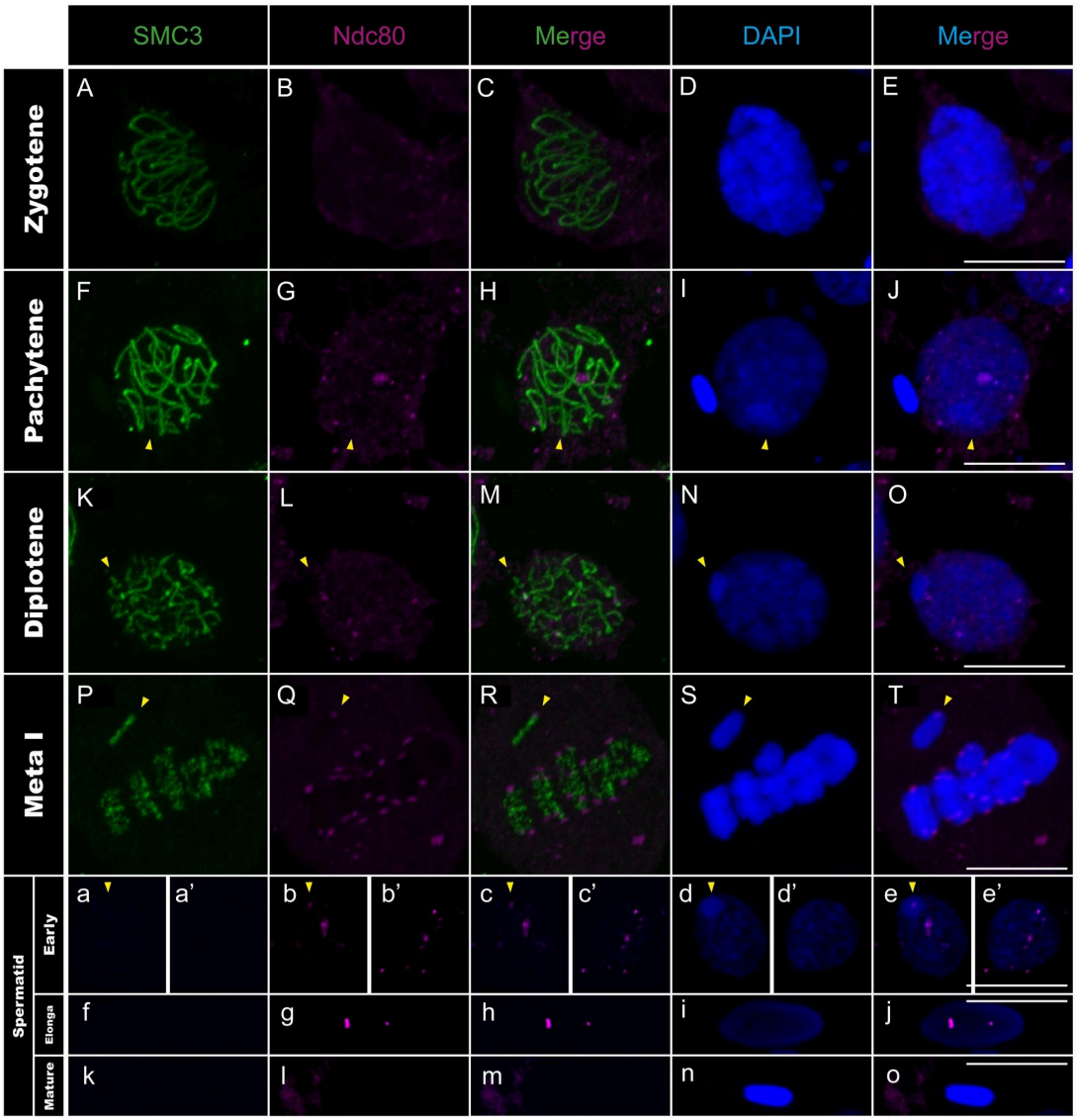

Figure 8: Ndc80 distribution in *T. californicum* meiocytes and spermatids. Projections of stack images acquired across *T. californicum* squashed meiocytes (A–T) and spermatids (a–o), at the stages indicated, stained with DAPI (blue) and double immunolabeled for SMC3 (green) and Ndc80 (magenta). Ndc80 signal is not detected until the pro-metaphase I stage (see Supplemental figure 8) where it is distributed in foci on every chromosome until anaphase II (see Supplemental figure 8). The Ndc80 signal is then lost from centromeres at the onset of spermiogenesis, although two to three regions (likely non-centromeric, see main text) appear positive for Ndc80 in round and elongated spermatids. The position of the sex (X) chromosome is indicated with arrowheads. Scale bar: 10 µm.

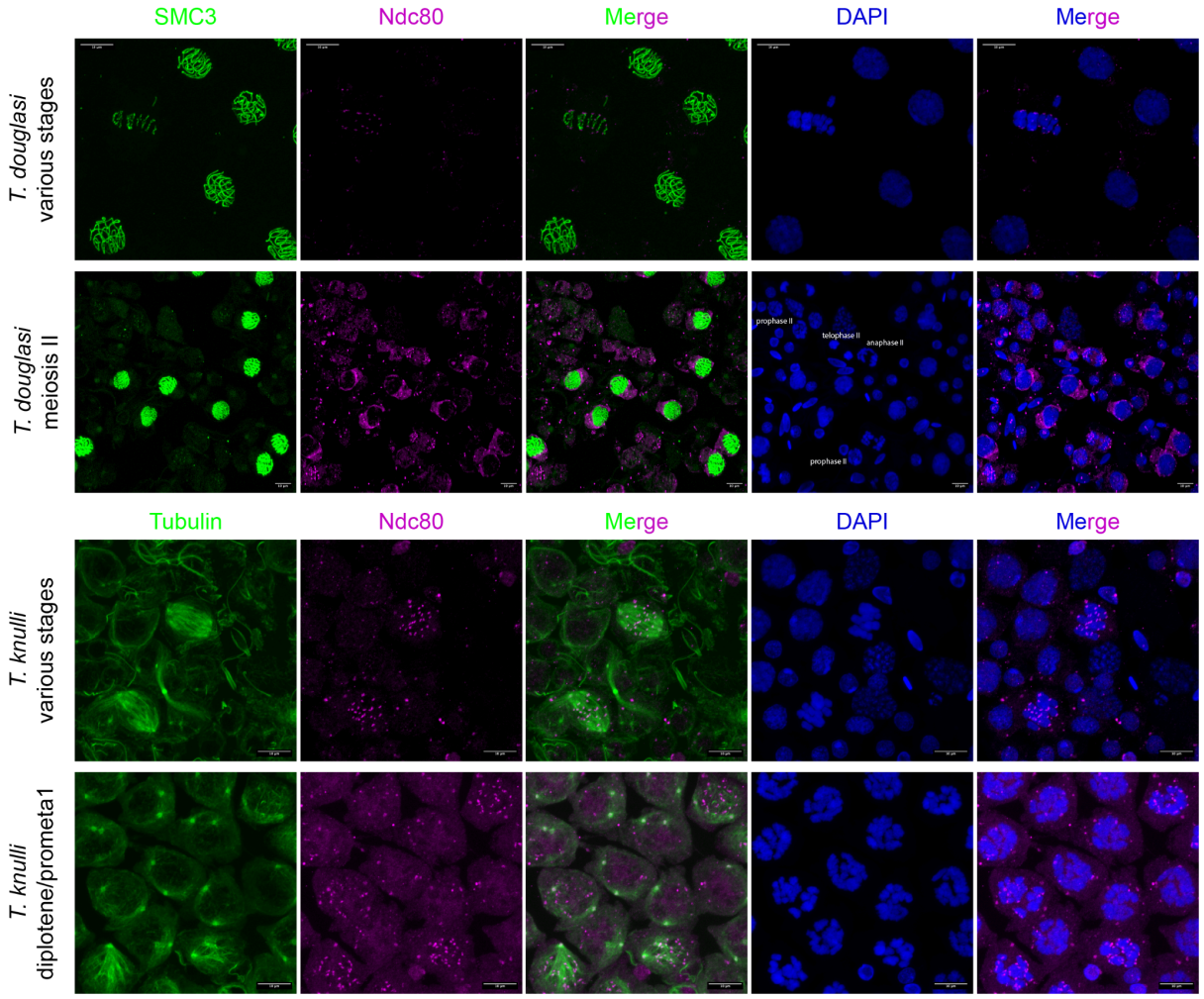

Supplemental figure 8: Ndc80 distribution in various stages of spermatogenesis for two additional species, acquired through the projection of stack images. Scale bar: 10 µm.

During the second meiotic division, CenpC and Bub1 are found to localize to centromeres and to detach rapidly after, as evidenced by the loss of signals towards the end of the second meiotic division (Figure 7; Figure 9; Supplemental figure 7; Supplemental figure 9). However, Ndc80 displays a surprising cellular pattern after meiosis, accumulating in a few regions until the formation of mature sperm cells (Figure 8; Supplemental figure 8). Although this cellular localization remains unexplained, it is very unlikely to reflect a clusterization of centromeres

as they appear distinctly visible when marked with the CenH3 protein at this stage (Figure 6; Supplemental figure 6).

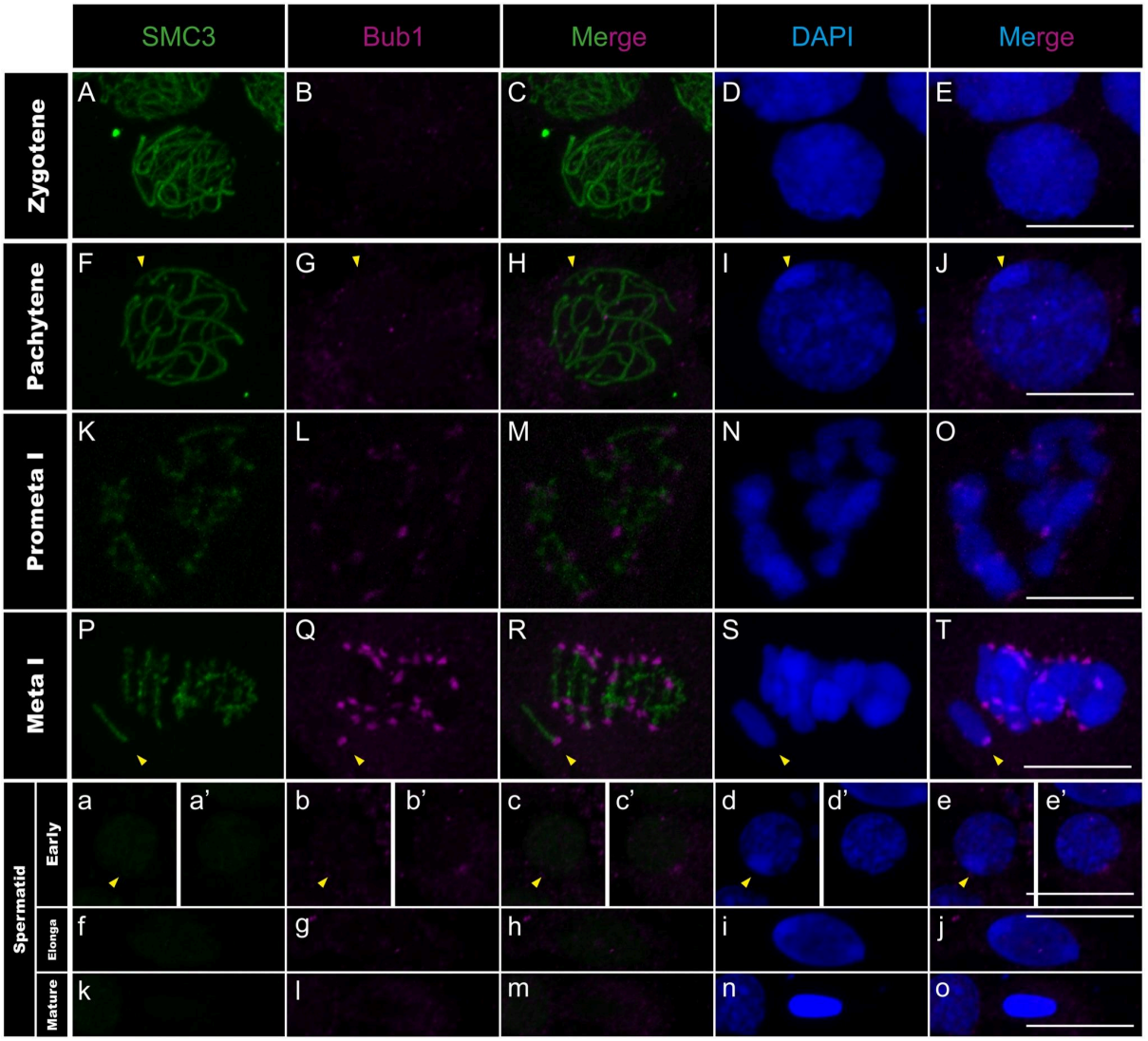

Figure 9: Bub1 distribution in *T. californicum* meiocytes and spermatids. Projections of stack images acquired across *T. californicum* squashed meiocytes (A–T) and spermatids (a–o), in the stages indicated, stained with DAPI (blue) and double immunolabeled for SMC3 (green) and Bub1 (magenta). Bub1 signal is not detected until the prometaphase I stage where it is distributed in foci on every chromosome until anaphase II (see Supplemental figure 9). The Bub1 signal is then lost at

the onset of spermiogenesis. The position of the sex (X) chromosome is indicated with arrowheads. Scale bar: 10 µm.

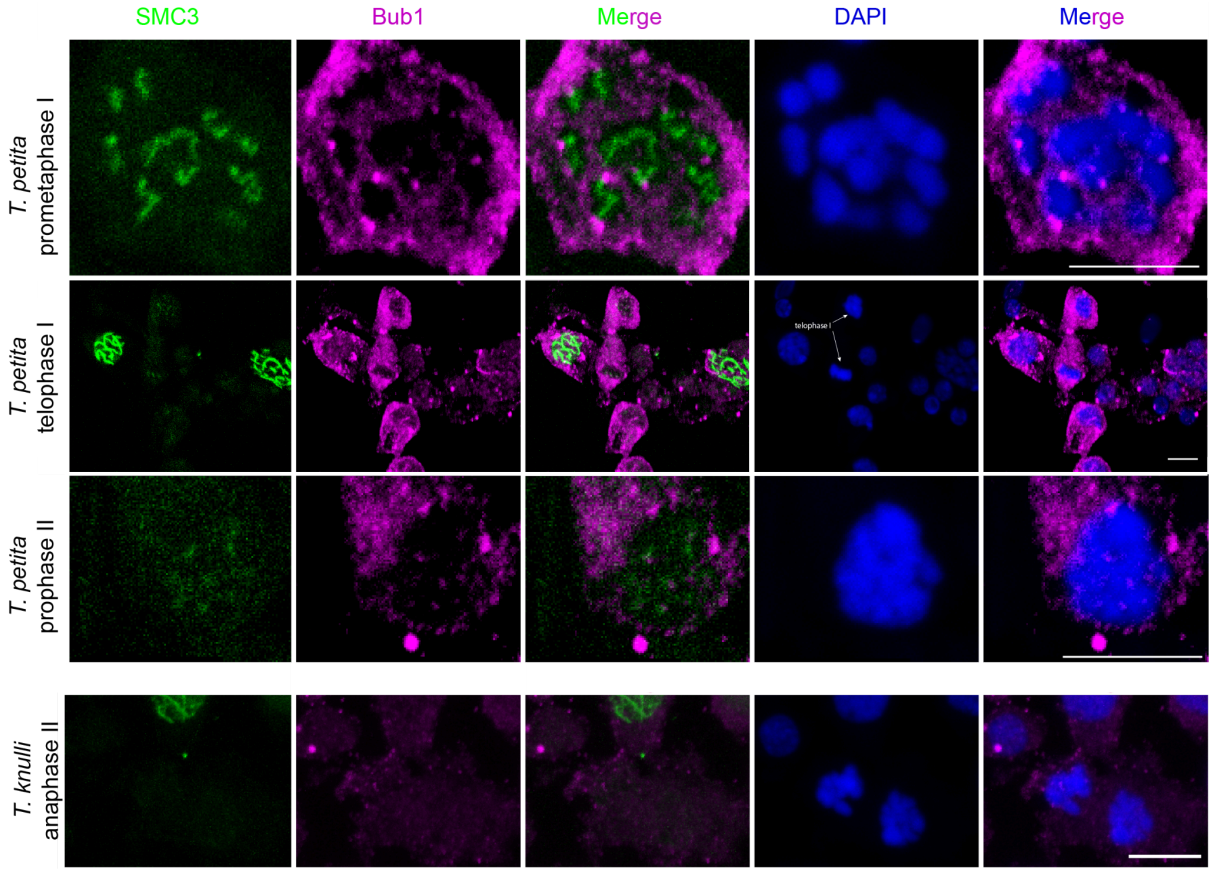

Supplemental figure 9: Bub1 distribution at various stages of spermatogenesis for two additional species, acquired through the projection of stack images. Scale bar: 10 µm.

Overall, our findings reveal that the recruitment of centromere proteins in *Timema* male meiosis is decoupled in space and time, following at least three main steps. Initially, CenH3 distributes along the entire length of all chromosomes while the other centromere proteins are absent. This is then followed by focal restriction of CenH3 on each autosome and monocentric recruitment of CenpC on all chromosomes (autosomes and the X chromosome) during synapsis. Just before the first cellular division, the last components of the kinetochore

and SAC proteins are recruited in monocentric fashion, forming the active centromere that attaches to spindle microtubules during metaphase I (Toubiana et al. 2024). By the end of the second meiotic division, kinetochore and SAC complexes disassemble and leave the centromere regions with only the CenH3 proteins.

Taken together, this study represents one of the rare instances describing the cellular dynamics of essential centromere proteins during male meiosis, building also upon previous research on univalent chromosome segregation in praying mantis and grasshoppers (47-50).

The regulation and dynamics of chromosomes during spermatogenesis is essential for male reproductive success. Yet, the mechanisms underlying these chromosomal events and how they evolve across species remains poorly understood. Our data offer new insights in this regard, identifying new dynamics and evolutionary patterns associated with chromosome segregation and X meiotic silencing, while supporting the idea that recombination preceding synapsis is an ancestral state in insects. Collectively, this study emphasizes the need to go beyond established model systems in cell biology to embrace the diversity of mechanisms underlying male gamete formations and provide the sufficient knowledge to understand the questions associated with inheritance and its evolution.

MATERIAL AND METHODS

Timema Sample Collection

We used wild-collected individuals of the species *T. douglasi* (38°57'24.9"N 123°32'10.0"W), *T. knulli* (35°50'10.3"N 121°23'29.3"W), *T. petita* (36°21'32.0"N 121°54'01.3"W), *T. californicum* (37°20'35.4"N 121°38'11.3"W), *T. cristinae* (34°32'25.4"N 119°14'20.5"W), *T. monikensis* (34°06'53.6"N 118°51'11.3"W), *T. bartmani* (34°09'48.1"N 116°51'43.5"W) and *T. chumash* (34°06'53.6"N 118°51'11.3"W).

Design and selection of antibodies

A combination of custom and commercially available antibodies was employed for the immunostaining assays (Supplemental table 1). Details of the custom antibody designs for Timema CenH3 and kinetochore proteins can be found in Toubiana et al. 2024 and in the Supplemental table 1. For the SAC protein Bub1, we first used the protein sequence of *Drosophila melanogaster* to identify orthologs in stick insects via Protein BLAST against the NCBI database. A blast hit was already annotated as Bub1 in the stick insect *Bacillus rossius redtenbacheri* (XP_063234342.1) and was further used to identify orthologs in *Timema* via Protein BLAST against the NCBI database. The best hits of nine *Timema* species corresponded to the Bub1 ortholog as revealed by Protein BLAST against the non-redundant NCBI database. We then used the protein sequence from *T. poppense* (CAD7396045.1) to outsource to Covalab (Lyon, France) the design of three distinct peptide

sequences (Supplemental table 1). Covalab subsequently developed polyclonal rabbit antibodies for the target gene using the designed peptides, and purified them via a sepharose column.

List of primary custom antibodies				
Short Name	**Company**	**Clonality**	**Host**	**Peptide sequence**
Bub1	Covalab	Polyclonal	Rabbit	C-EADNPIVYQELIKEQQRYE-coNH2
				C-EFSLEELRAIIYNKKYEEK-coNH2
				C-HPAIPSRPEEKSGPLQPST-coNH2

List of primary commercial antibodies				
Short Name	**Ref**	**Company**	**Final Concentration**	**Conjugated / Host**
SMC3	ab201542	AbCam	1:100	Alexa Fluor 488 / Rabbit
RNA Pol II	ab193468	AbCam	1:100	No / Rabbit
H3K9me3	ab8898	AbCam	1:100	No / Rabbit
RAD51	PC130	Sigma-Aldrich	1:70	No / Rabbit
γH2AX	05-636	Sigma-Aldrich	1:200	No / Rabbit
α_Tubulin	#F2168	Sigma-Aldrich	1:150	FITC / Mouse

List of secondary antibodies				
Short Name	**Ref**	**Company**	**Final Concentration**	**Conjugated**
anti-Rabbit-Alexa 594	711-585-152	Jackson	1:150	Alexa Fluor 594

Chemicals used for immuno-staining				
Name	**Ref**	**Company**	**Working Solution**	
DAPI	D9542	Sigma-Aldrich	10ug/mL	
Normal Rabbit Serum (NRS)	X090210-8	Agilent Technonoly	5% in PBS 1x (v/v)	
Vectashield Mounting Medium	H1000	ReactoLab		

Supplemental table 1: Antibodies and chemicals used. A combination of custom and commercially available antibodies was employed for the immunostaining assays.

Immunostaining procedure with SMC3 antibody

Male gonads display a morphology resembling grapes, comprising a shoot housing mature sperm cells and an oval structure encapsulating cells at various meiotic stages (see Toubiana et al. 2024). Gonads from alive adults were dissected in 1X PBS, fixed in a solution containing 2% paraformaldehyde and 0.1% Triton X-100 for 15 minutes, followed by gentle squashing of 4-5 "grapes" onto poly-L-lysine-coated slides, then rapidly immersed in liquid nitrogen (according to (51)). After a 20-minute incubation in 1X PBS, tissues on slides were subjected to blocking with 3% BSA (in 1X PBS (w/v)) blocking buffer for a minimum of 30 minutes.

Immunostaining started by incubating slides with diluted primary antibodies in 3% BSA overnight at 4°C within a humid chamber. Exception was made for the already fluorescently labeled SMC3 antibody that was added after the following blocking step (see below). Detailed information for all antibodies used, including working concentrations, are provided in Supplemental table 1. Subsequently, slides underwent three 5-minutes washes in 1X PBS, followed by a 1-hour incubation with the secondary antibody, diluted at a ratio of 1:150 in 3% BSA, at room temperature. Slides were then washed thrice for 5 minutes each, followed by a 10-minute wash in 1X PBS.

As most primary antibodies were developed from the same host (i.e. rabbit), a blocking step was performed using diluted Normal Rabbit Serum (NRS 5%) for 30 minutes at room temperature, followed by a 10-minute wash in 1X PBS. Subsequently, slides underwent a 1-hour incubation at

room temperature with the already fluorescently labeled SMC3 antibody diluted at 1:100. Slides were washed thrice in 1X PBS, stained with DAPI for 3 minutes, washed one last time 5 minutes in 1X PBS, and mounted in Vectashield media.

Immunostaining procedure without SMC3 antibody

For this procedure, no blocking steps (i.e. without 3% BSA and NRS) were performed. Therefore, after a 20-minute incubation in PBS, tissues on slides were directly incubated with diluted primary antibodies in 1X PBS overnight at 4°C within a humid chamber. Exception was made for the already fluorescently labeled α-tubulin antibody that was used in the following step (with the secondary antibody). Slides were then washed thrice for 5 minutes each in 1X PBS, followed by a 1-hour incubation with the secondary antibody (Alexa-Fluor-594) or the already fluorescently labeled α-tubulin antibody (when needed), diluted at a ratio of 1:150 in 1X PBS, at room temperature. Slides were washed thrice in 1X PBS, stained with DAPI for 3 minutes, washed one last time 5 minutes in 1X PBS, and mounted in Vectashield media.

Image acquisition

All acquisitions were performed using the Zeiss LSM 880 airyscan confocal microscope equipped with a 60x/oil immersion objective. All acquisitions were produced by the superimposition of focal planes. Post-processing, including cropping and pseudocoloring, was carried out using Fiji (52).

Acknowledgement

We thank current and previous members of the Schwander lab for discussions. We also thank Rocío Gómez for help in developing the immunostaining protocol in *Timema*, and Arnaud Paradis from Cell Imaging Facility (CIF, Lausanne University, Switzerland) for his help with image acquisitions. **Funding**: We would like to acknowledge funding from the European Research Council Consolidator Grant (No Sex No Conflict to T.S.) and Swiss FNS grant 31003A_182495 (T.S.). **Author contributions**: Z.D., W.T. and T.S. designed the study. Z.D. and W.T. performed molecular work. Z.D. developed methods. Z.D. and W.T. analyzed the data with input from T.S.. Z.D., W.T. and T.S. wrote the paper.

REFERENCES

1. Zickler D, Kleckner N. Meiosis: Dances Between Homologs. Annu Rev Genet. 2023;57:1-63.
2. Hao SL, Ni FD, Yang WX. The dynamics and regulation of chromatin remodeling during spermiogenesis. Gene. 2019;706:201-10.
3. Lenormand T, Engelstädter J, Johnston SE, Wijnker E, Haag CR. Evolutionary mysteries in meiosis. Philos T R Soc B. 2016;371(1706).
4. Loidl J. Conservation and Variability of Meiosis Across the Eukaryotes. Annual Review of Genetics, Vol 50. 2016;50:293-316.
5. White-Cooper H, Bausek N. Evolution and spermatogenesis. Philos T R Soc B. 2010;365(1546):1465-80.
6. T. SKONE. Achiasmy and sex chromosome evolution. Ecological Genetics and Genomics. 2019.
7. Jang JK, Sherizen DE, Bhagat R, Manheim EA, McKim KS. Relationship of DNA double-strand breaks to synapsis in Drosophila. J Cell Sci. 2003;116(15):3069-77.
8. Viera A, Santos JL, Page J, Parra MT, Calvente A, Cifuentes M, et al. DNA double-strand breaks, recombination and synapsis:: the timing of meiosis differs in grasshoppers and flies. Embo Rep. 2004;5(4):385-91.
9. Parker DJ, Jaron KS, Dumas Z, Robinson-Rechavi M, Schwander T. X chromosomes show relaxed selection and complete somatic dosage compensation across stick insect species. J Evolution Biol. 2022;35(12).
10. Revenkova E, Jessberger R. Keeping sister chromatids together: cohesins in meiosis. Reproduction. 2005;130(6):783-90.
11. Scherthan H. A bouquet makes ends meet. Nat Rev Mol Cell Bio. 2001;2(8):621-7.
12. Mahadevaiah SK, Turner JMA, Baudat F, Rogakou EP, de Boer P, Blanco-Rodríguez J, et al. Recombinational DNA double-strand breaks in mice precede synapsis. Nat Genet. 2001;27(3):271-6.
13. Kleckner N. Meiosis: How could it work? P Natl Acad Sci USA. 1996;93(16):8167-74.
14. Grelon M, Vezon D, Gendrot G, Pelletier G. AtSPO11-1 is necessary for efficient meiotic recombination in plants. Embo J. 2001;20(3):589-600.
15. Viera A, Parra MT, Arevalo S, de la Vega CG, Santos JL, Page J. X Chromosome Inactivation during Grasshopper Spermatogenesis. Genes-Basel. 2021;12(12).
16. Viera A, Santos JL, Parra MT, Calvente A, Gómez R, de la Fuente R, et al. Cohesin axis maturation and presence of RAD51 during first meiotic prophase in a true bug. Chromosoma. 2009;118(5):575-89.
17. Holm PB, Rasmussen SW. Chromosome-Pairing, Recombination Nodules and Chiasma Formation in Diploid Bombyx Males. Carlsberg Res Commun. 1980;45(6):483-548.
18. Cahoon CK, Libuda DE. Leagues of their own: sexually dimorphic features of meiotic prophase I. Chromosoma. 2019;128(3):199-214.
19. Ishiguro KI. Sexually Dimorphic Properties in Meiotic Chromosome. Sex Dev. 2023;16(5-6):423-33.
20. Furman BLS, Metzger DCH, Darolti I, Wright AE, Sandkam BA, Almeida P, et al. Sex Chromosome Evolution: So Many Exceptions to the Rules. Genome Biol Evol. 2020;12(6):750-63.
21. Daish TJ, Casey AE, Grutzner F. Lack of sex chromosome specific meiotic silencing in platypus reveals origin of MSCI in therian mammals. Bmc Biol. 2015;13.

22. Guioli S, Lovell-Badge R, Turner JMA. Error-Prone ZW Pairing and No Evidence for Meiotic Sex Chromosome Inactivation in the Chicken Germ Line. Plos Genet. 2012;8(3).
23. Namekawa SH, VandeBerg JL, McCarrey JR, Lee JT. Sex chromosome silencing in the marsupial male germ line. P Natl Acad Sci USA. 2007;104(23):9730-5.
24. Page J, de la Fuente R, Manterola M, Parra MT, Viera A, Berríos S, et al. Inactivation or non-reactivation: what accounts better for the silence of sex chromosomes during mammalian male meiosis? Chromosoma. 2012;121(3):307-26.
25. Turner JMA. Meiotic sex chromosome inactivation. Development. 2007;134(10):1823-31.
26. Cloutier JM, Turner JMA. Meiotic sex chromosome inactivation. Curr Biol. 2010;20(22):R962-R3.
27. Ichijima Y, Sin HS, Namekawa SH. Sex chromosome inactivation in germ cells: emerging roles of DNA damage response pathways. Cell Mol Life Sci. 2012;69(15):2559-72.
28. Handel MA. The XY body: a specialized meiotic chromatin domain. Exp Cell Res. 2004;296(1):57-63.
29. Viera A, Calvente A, Page J, Parra MT, Gómez R, Suja JA, et al. X and B chromosomes display similar meiotic characteristics in male grasshoppers. Cytogenet Genome Res. 2004;106(2-4):302-8.
30. Viera A, Parra MT, Rufas JS, Page J. Transcription reactivation during the first meiotic prophase in bugs is not dependent on synapsis. Chromosoma. 2017;126(1):179-94.
31. Turner JMA. Meiotic Silencing in Mammals. Annual Review of Genetics, Vol 49. 2015;49:395-412.
32. MacQueen AJ, Hochwagen A. Checkpoint mechanisms: the puppet masters of meiotic prophase. Trends Cell Biol. 2011;21(7):393-400.
33. Namekawa SH, Park PJ, Zhang LF, Shima JE, McCarrey JR, Griswold MD, et al. Postmeiotic sex chromatin in the male germline of mice. Curr Biol. 2006;16(7):660-7.
34. McKinley KL, Cheeseman IM. The molecular basis for centromere identity and function. Nat Rev Mol Cell Bio. 2016;17(1).
35. Senaratne AP, Cortes-Silva N, Drinnenberg IA. Evolution of holocentric chromosomes: Drivers, diversity, and deterrents. Semin Cell Dev Biol. 2022;127:90-9.
36. Gassmann R, Rechtsteiner A, Yuen KW, Muroyama A, Egelhofer T, Gaydos L, et al. An inverse relationship to germline transcription defines centromeric chromatin in C. elegans. Nature. 2012;484(7395):534-U166.
37. Senaratne AP, Muller H, Fryer KA, Kawamoto M, Katsuma S, Drinnenberg IA. Formation of the CenH3-Deficient Holocentromere in Lepidoptera Avoids Active Chromatin. Curr Biol. 2021;31(1):173-+.
38. Kursel LE, McConnell H, de la Cruz AFA, Malik HS. Gametic specialization of centromeric histone paralogs in Drosophila virilis. Life Sci Alliance. 2021;4(7).
39. Câmara AS, Schubert V, Mascher M, Houben A. A simple model explains the cell cycle-dependent assembly of centromeric nucleosomes in holocentric species. Nucleic Acids Res. 2021;49(16):9053-65.
40. Müller S, Almouzni G. A network of players in H3 histone variant deposition and maintenance at centromeres. Bba-Gene Regul Mech. 2014;1839(3):241-50.
41. Fellmeth JE, McKim KS. Meiotic CENP-C is a shepherd: bridging the space between the centromere and the kinetochore in time and space. Essays Biochem. 2020;64(2):251-61.
42. Mellone BG, Fachinetti D. Diverse mechanisms of centromere specification. Curr Biol. 2021;31(22):R1491-R504.

43. Musacchio A, Desai A. A Molecular View of Kinetochore Assembly and Function. Biology-Basel. 2017;6(1).
44. Musacchio A, Salmon ED. The spindle-assembly checkpoint in space and time. Nat Rev Mol Cell Bio. 2007;8(5):379-93.
45. Gorbsky GJ. The spindle checkpoint and chromosome segregation in meiosis. Febs J. 2015;282(13):2458-74.
46. Miller MP, Ünal E, Brar GA, Amon A. Meiosis I chromosome segregation is established through regulation of microtubule-kinetochore interactions. Elife. 2012;1.
47. Li XT, Nicklas RB. Tension-sensitive kinetochore phosphorylation and the chromosome distribution checkpoint in praying mantid spermatocytes. J Cell Sci. 1997;110:537-45.
48. Nicklas RB, Ward SC, Gorbsky GJ. Kinetochore Chemistry Is Sensitive to Tension and May Link Mitotic Forces to a Cell-Cycle Checkpoint. J Cell Biol. 1995;130(4):929-39.
49. Nicklas RB, Waters JC, Salmon ED, Ward SC. Checkpoint signals in grasshopper meiosis are sensitive to microtubule attachment, but tension is still essential. J Cell Sci. 2001;114(23):4173-83.
50. Parra MT, Gómez R, Viera A, Llano E, Pendás AM, Rufas JS, et al. Sequential Assembly of Centromeric Proteins in Male Mouse Meiosis. Plos Genet. 2009;5(3).